HHS Public Access

Author manuscript

Dev Dyn. Author manuscript; available in PMC 2024 September 01.

Published in final edited form as:

Dev Dyn. 2023 September ; 252(9): 1180–1188. doi:10.1002/dvdy.600.

Loss of *Fgfr1* and *Fgfr2* in Scleraxis-lineage cells leads to enlarged bone eminences and attachment cell death

Kendra K. Wernlé[1,2], **Michael A. Sonnenfelt**[1], **Connor C. Leek**[1,3], **Elahe Ganji**[1,3,4], **Anna Lia Sullivan**[1], **Claudia Offutt**[1], **Jordan Shuff**[1], **David M. Ornitz**[5], **Megan L. Killian**[1,3]

[1.]Department of Biomedical Engineering, University of Delaware, 150 Academy St, Newark, Delaware, 19716

[2.]Institute of Anatomy, University of Zürich, Winterthurerstrasse 190, Zürich, Switzerland

[3.]Department of Orthopaedic Surgery, University of Michigan, 109 Zina Pitcher Pl, Ann Arbor, MI 48109

[4.]Department of Mechanical Engineering, University of Delaware, 130 Academy St, Newark, DE 19716

[5.]Department of Developmental Biology, Washington University School of Medicine, 660 S. Euclid Avenue, St Louis, Missouri, 63110

Abstract

Background: Tendons and ligaments attach to bone are essential for joint mobility and stability in vertebrates. Tendon and ligament attachments (i.e., entheses) are found at bony protrusions (i.e., eminences), and the shape and size of these protrusions depends on both mechanical forces and cellular cues during growth. Tendon eminences also contributes to mechanical leverage for skeletal muscle. Fibroblast growth factor receptor (FGFR) signaling plays a critical role in bone development, and *Fgfr1* and *Fgfr2* are highly expressed in the perichondrium and periosteum of bone where entheses can be found.

Results and Conclusions: We used transgenic mice for combinatorial knockout of *Fgfr1* and/or *Fgfr2* in tendon/attachment progenitors (ScxCre) and measured eminence size and shape. Conditional deletion of both, but not individual, *Fgfr1* and *Fgfr2* in *Scx* progenitors led to enlarged eminences in the postnatal skeleton and shortening of long bones. In addition, *Fgfr1/Fgfr2* double

Corresponding author: Megan L. Killian, PhD mlkillia@med.umich.edu.

Author contributions:
Conceptualization: Lead- DMO and MLK; Supporting- KKW and MAS
Data curation: Lead- KKW, MAS, and MLK; Supporting- CCL, EG, ALS
Formal analysis: Lead- KKW, MAS, CCL, MLK; Supporting- EG, CO, JS
Funding acquisition: Lead- MLK; Supporting- DMO
Investigation: Lead- KKW, MAS, CCL, MLK; Supporting- EG, ALS, CO, JS
Methodology: Lead- KKW, MAS, CCL, MLK; Supporting- EG, ALS, DMO
Project administration: Lead- KKW, MLS, MLK
Resources: Lead- MLK
Software: Lead- KKW, MAS, CCL, MLK
Supervision: Lead- MLK
Validation: Lead- KKW, MAS, CCL, MLK
Visualization: Lead- KKW, MAS, CCL, MLK; Supporting- DMO, EG, ALS, CO
Writing- original draft: Lead- KKW, MAS, MLK; Supporting- CCL, EG, DMO
Writing- review and editing: Lead- KKW, MAS, MLK; Supporting- CCL, EG, ALS, CO, JS, DMO

conditional knockout mice had more variation collagen fibril size in tendon, decreased tibial slope, and increased cell death at ligament attachments. These findings identify a role for FGFR signaling in regulating growth and maintenance of tendon/ligament attachments and the size and shape of bony eminences.

Introduction

Tendons and ligaments transmit mechanical forces to bone and are essential for joint mobility and stability in vertebrates (1–3). During development, the attachments of most tendons and ligaments of the appendicular skeleton mature into graded fibrocartilage interfaces between tendon/ligament and bone (2,4–6). These fibrocartilage attachments are often found at bone eminences, which are superstructures on the periosteal surface of bone such as tuberosities and tubercles, that increase leverage between the line of action of applied mechanical force (e.g., skeletal muscle) and the center of a joint (7–9). In mice, eminence formation initiates around embryonic day (E)12.5 from a recruited progenitor pool that co-expresses *Scleraxis* (*Scx*) and *Sox9* and surrounds the cartilage anlage of developing bone (7,10). Eminences form “miniature” growth plates at tendon/ligament attachments and follow similar developmental patterns to the primary growth plate during longitudinal bone growth (1,8,9,11–14). In the absence of muscle loading, such as paralysis, chondrocyte proliferation within the mini-growth plate of the developing eminence is arrested (8). In addition, the absence of muscle loading also leads to malformed synovial joints in embryonic limbs (15–22). However, it remains unclear if and how growth and shape of tendon and ligament attachments are regulated by similar molecular cues to the growth plate.

Fibroblast growth factors (FGFs) play a critical role in bone development and maturation (23). FGF ligands bind with high affinity to transmembrane tyrosine kinase receptors, FGFRs, and these ligands and receptors directly interact with heparan sulfate proteoglycans (23), which are richly deposited during cartilage development as well as at sites of tendon and ligament attachments (24). Recent work has demonstrated cell-specific mechanisms of both *Fgfr1* and *Fgfr2* signaling in long bone development (25,26). Expression of *Fgfr1* is localized to the hypertrophic chondrocytes of the developing growth plate, and both *Fgfr1* and *Fgfr2* are highly expressed in the perichondrium and periosteum (23). Loss of *Fgfr1* and *Fgfr2* in osteoprogenitor cells results in increased expression of *Fgfr3* and *Fgf9* and the non-autonomous regulation of growth plate chondrocytes, leading to suppressed chondrocyte proliferation and shorter bones (25). In mice lacking *Fgfr1* expression in mature osteoblasts and osteocytes, the osteocytes die resulting in secondary bone overgrowth (26). Surprisingly, although global deletion of *Fgf9* leads to shortened bones as well, developing eminences of the humerus (e.g., deltoid tuberosity) becomes noticeably enlarged (27–29). This differential regulation of growth between long bone growth plates and eminence “mini” growth plates led us to further explore the role that FGFR signaling plays in the size and shape of tuberosities. Recently, work by Roberts et al. showed that deletion of *Fgfr2* in neural crest cells leads to smaller eminences in the craniofacial complex (30). Yet the link between FGFR signaling and postnatal eminence maturation in the appendicular skeleton remains unclear.

In this study, we show that eminence growth and maintenance in the mammalian limb is regulated in part by FGFR signaling. Loss of *Fgfr1* and *Fgfr2* in tendon/ligament progenitors led to unrestricted growth of eminences in the appendicular skeleton and increased cell death at ligament attachments. These results identify a critical role of FGFR signaling in regulating growth and maintenance of tendon/ligament attachments at eminences for controlling the shape and structure of bones.

Results

Scx-lineage targets tendon/ligament and attachments

Lineage tracing experiments showed consistent localization of ScxCre; *ROSA*^{tdTomato} (Ai14) cells (*Scx*Cre tdTomato+ lineage) in tendons, ligaments, and entheses (Figure 1). Additionally, tdTomato+ cells were found within the secondary ossification center of bone (at ~3-4 weeks of age) and the mineralized zone of the growth plate, similar to the *Osx*-Cre lineage (33,34). TdTomato+ cells from the ScxCre; *ROSA*^{tdTomato} lineage were prevalent in the perichondrium surrounding the proximal and distal sites of the secondary ossification centers, which differs from previous reports using lineage tracing of mesenchymal progenitors (e.g., *Osx*-Cre; Figure 1) (35). Also, unlike *Osx*-Cre lineage tracing, *Scx*Cre tdTomato+ cells were localized to tendon, ligament, articular cartilage, and other fibrous/fibrocartilaginous connective tissues (e.g., meniscus).

ScxCre-DKO mice had larger tuberosities, yet shorter bones, compared to WT littermates

There were no gross phenotypic differences at the time of weaning between WT and DKO mice; however, DKO mice weighed less (15.9 ± 2.34g, n=5) compared to WT mice (18.9 ± 1.99g, n=6; $p<0.05$) at 8 weeks of age. R1cKO and R2cKO mice were comparable to WT (R1cKO: 22.03 ± 4.90g, n = 3 and R2cKO: 18.2 ± 5.30g, n = 3). DKO mice consistently had shorter bones compared to WT mice at 8 weeks and 6 months of age (Figure 2A). Despite DKO mice having shorter humeri, tuberosities on the humeri (the deltoid tuberosity, DT; and lateral supracondylar ridge, LSR) were significantly larger in DKO mice compared to WT mice at 6 months of age (Figure 2B). This enlarged tuberosity phenotype was also observed at sites of tendon attachments in the tibia (Figure 3).

DKO mice had decreased tibial slope and increased cell death at ligament entheses in the knee

Based on the distinct phenotype related to increased tuberosity size in adult DKO mice, we also investigated the shape and morphometry of articular joints, specifically the knee. DKO mice had reduced tibial slope compared to WT littermates at 6-8 months (Figure 4A). Single receptor mutants (*Fgfr1* or *Fgfr2* cKO) did not have any remarkable bone phenotypes when compared to DKO mice, with comparable tibia lengths to WT mice at 6-8 months of age (Figure 3). Tibial cortical bone mineral density (BMD) was significantly lower in DKO mice (1,090 ± 66mg HA/cm^3) compared to WT mice (1,167 ± 50mg HA/cm^3) at 6-8 months of age.

The tibia slope was significantly reduced in the medial compartment of DKO mice at 6-8 months of age compared to WT mice (Figure 4A). Histologically, the patella and proximal

patellar tendon appeared smaller in DKO mice compared to WT mice at 3 weeks of age (Figure 4B,C). Additionally, the groove of Ranvier, denoted by germinal-like cells adjacent to the growth plate, was also smaller (Figure 4B',C').

Based on these morphological findings, we further investigated DNA damage and cell death at the attachment site of the intraarticular ligaments of the knee. Attachment sites of cruciate ligaments in 3-week-old DKO knees had significantly increased cell apoptosis, indicated by increased TUNEL+ staining, compared to attachment sites in age-matched WT knees (Figure 5). The number of cells analyzed were similar between WT (202 ± 49 cells) and DKO (208 ± 83 cells) attachments, however there were significantly more TUNEL+ cells in the DKO attachments (23 ± 10 cells) compared to WT attachments (3 ± 1 cells). Apoptotic cells were primarily localized to the mineralizing region of the interface and were not found in the fibrous ligament tissue (Figure 5). No other regions in histological sections of the mouse knee had a remarkable presentation of apoptotic cells.

Increased collagen fibril size in DKO compared to WT Achilles tendons

The ultrastructural properties of tendon collagen fibrils were analyzed in the Achilles tendon at 6-8 months of age in WT and DKO mice (Figure 6A,B). DKO mice had a higher frequency of small fibrils in Achilles tendon compared to WT mice (~40-50nm diameter) and also had more larger collagen fibrils compared to WT (~260-300nm; Figure 6C). The relative area covered by collagen fibrils was higher in DKO tendons compared to WT tendons (Figure 6D), but the average fibril area was not significantly different between groups (Figure 6F).

Discussion

Each bone in the adult mammalian skeleton has a unique shape and structure that accommodates its functional requirements for movement and stability. The formation of superstructures along the surface gives bone their unique shape and provide distinct attachment sites for tendons, yet the mechanism by which these superstructures grow has only recently been explored (8). In this study, we showed that FGF signaling plays a role in regulating the shape and structure of these superstructures in the mature skeleton. We discovered that ablation of FGF signaling in developing tendon and attachments results in aberrant bone shape, such as enlarged mineralized superstructures, and alters the ultrastructure of tendon collagen fibrils. These changes in the structural properties may influence functional outcomes, such as joint movement. From these studies, it remains unclear if the tendon ultrastructure was a primary outcome of altered FGF signaling or if these changes were caused by a secondary effect of altered tendon loading induced by irregular joint shape and more mechanistic studies of the developing tendon and enthesis are needed. Nonetheless, deletion of *Fgfr1* and *Fgfr2* in *Scx*-lineage cells may lead to impaired expansion of secondary ossification centers in long bones, resulting in shorter bones and flattened epiphyses, which can be observed in histology (e.g., Figure 4). McKenzie et al. recently described increased osteocyte death in mice lacking *Fgfr1* and *Fgfr2* either in osteoblasts or osteocytes that led to increased cortical remodeling and bone accrual (26). We also found increased cell death in the subchondral region, but not the ligamentous region,

of ligament attachments in the knees of young ScxCre-DKO mice, which may have directly or indirectly caused increased bone apposition at the enthesis. The cells responsible for maintenance of this mineralized region of the ligament attachment may be derived from cells from both the *Scx* lineage and cells that are hedgehog-responsive (e.g., Gli1+) (13). Further investigation into the mechanism by which enthesis progenitors are maintained and how FGF signaling regulates cell survival and bone accrual at the enthesis are needed.

In connective tissue (i.e., tendon), ultrastructural analysis showed that some DKO collagen fibrils were larger and their size distribution differed compared to normal collagen fibrils in WT tendons. The size and structure of collagen fibrils in tendon is controlled by small leucine-rich proteoglycans (e.g., decorin) containing glycosaminoglycan chains of either chondroitin sulfate or dermatan sulfate. Ablation of decorin and its complimentary protein, biglycan, results in larger fibril diameter in tendons, similar to what we observed in ScxCre-DKO mice (36). Heparan sulfate proteoglycans (HSPG), which preferentially bind FGF ligands and receptors, may also regulate type I collagen fibrillogenesis (37,38), and additional work is needed to explore how HSPG regulates collagen fibril formation in both tendon and bone. Additionally, the differences in bone and joint morphometry may be related to age-dependent changes in collagen and extracellular matrix (ECM) organization, although this was not rigorously investigated in the current study.

Several ligands, including *Fgf2*, *Fgf9*, and *Fgf18*, are expressed in the perichondrium, and both FGF9 and FGF18 regulate chondrocyte hypertrophy in the growth plate by signaling to FGFR3 in chondrocytes (23). Activating mutations of FGFR3 cause achondroplasia, the most common skeletal dysplasia resulting in shortened and bowed lower limbs (39,40). Children with achondroplasia exhibit generalized joint hypermobility and weak muscle tone (41). It is possible that knockdown of *Fgfr1* and *Fgfr2* in our study led to a compensatory upregulation of *Fgfr3*, as has been demonstrated in previous ablation studies using skeletal promoters (Osx-Cre) (25).

This work is not without its limitations. Here, we studied the effect of tendon and attachment-specific ablation of FGF signaling by knocking out only two of the four FGF receptors, *Fgfr1* and *Fgfr2*. Additionally, we showed using lineage tracing that the Cre we used for these studies (ScxCre) targets a wider range of tissues than just tendon, ligament, and attachment sites (including chondrocytes). Although ScxCre *Fgfr1/Fgfr2* DKO adult mice had shortened bones, we do not expect this to be caused by primary growth plate disruptions, as ScxCre is not robustly expressed in proliferating or hypertrophic chondrocytes of the primary growth plate (8). Instead, such differences in bone length may be caused restricted growth plate expansion due to increased expression of FGF9/FGF18 and activation of FGFR3 (25). Even though DKO mice were smaller on average, the effect of partial FGFR signaling ablation resulting in enlarged bone ridges remains noteworthy.

In summary, we have shown that FGF signaling is an important regulator of bone shape and superstructure growth in the adult skeleton. FGF signaling may also play a role in cell survival and matrix remodeling at the tendon and ligament enthesis. The targeted disruption of FGF signaling in tendon and attachment progenitors led to phenotypic changes

in bone, joint, and enthesis morphology, including increased bone apposition and cell death at interfaces, underscoring its role in musculoskeletal growth and homeostasis.

Experimental Procedures

Animals

The University of Delaware Institutional Animal Care and Use Committee and Washington University Animal Care and Use Committee approved all animal use. Wild-type (WT) and *Fgfr* conditional knockout (KO) mice were bred in-house on a mixed C57BL/6J; 129X1 background in a specific pathogen-free facility and handled in accordance with standard use protocols and animal welfare regulations. A total of 79 mice were used for this study. Sample size of experimental and control groups varied based on breeding outcomes: $Fgfr1^{flx/flx};Fgfr2^{flx/flx}$ female mice were crossed with ScxCre;$Fgfr1^{flx/WT}$; $Fgfr2^{flx/WT}$ male mice to generate $ScxCre;Fgfr1^{flx/flx};Fgfr2^{flx/flx}$ mutants (DKO; n = 24; n = 3 at postnatal day 1 [P1]; n = 3 males and 4 females at 3-4 weeks of age; n = 2 males and 3 females at 8 weeks of age; and n = 5 males and 4 females at 6-8 months of age), as well as single mutants of $ScxCre;Fgfr1^{flx/flx};Fgfr2^{flx/WT}$ (R1cKO, n=3 males and 1 female at 6-8 months of age) and $ScxCre;Fgfr2^{flx/flx};Fgfr1^{flx/WT}$ (R2cKO, n=1 male and 1 female at 6-8 months of age). Cre-negative littermates were used as WT controls (n = 28; n = 3 males and 3 females at P1; n = 3 males and 5 females at 3-4 weeks of age; n = 3 males and 3 females at 8 weeks of age; and n = 4 males and 4 females at 6-8 months of age). Homozygous $ROSA^{tdTomato}$ (Ai14) reporter mice (Madisen, 2010, PMID: 20023653) (Jackson Laboratory, Bar Harbor, Maine) were crossed with ScxCre mice to generate ScxCre; $ROSA^{tdTomato}$ reporter mice (n = 20, mixed sex and ages). ScxCre mice were a gift from Ronen Schweitzer (Shriners Hospital for Children, Portland, OR) (8).

Lineage tracing

Knees of ScxCre; $ROSA^{tdTomato}$ reporter mice were dissected at the time of euthanasia (three time points: postnatal day 1-2; 2 weeks of age; or 2 months of age) and fixed in 4% paraformaldehyde for lineage tracing experiments. Tissues were decalcified in 14% EDTA for 2 weeks, embedded in SCEM (Section-Labs, Japan) or OCT (Fisher Scientific), and sectioned at 10μm. Sections were stained with DAPI (Vector Labs, CA, USA) and imaged on an inverted epifluorescent microscope (Zeiss AxioObserver Z1, Thornwood, NY).

Micro-computed tomography

Left hindlimbs and forelimbs of young adult mice at 8 weeks of age (n = 6 WT; n = 5 DKO) and adult mice at 6-8 months of age (n = 5 WT; n = 6 DKO; n = 4 R1cKO; n = 2 R2cKO) were fixed in 4% paraformaldehyde for 24-48 hr. Limbs were scanned using micro-computed tomography (microCT; Scanco Micro35, Switzerland; 20μm voxel size, 55kV, 72μA, 300ms integration time). Tibial length and bone mineral density of the cortex, as well as humeral length, epiphyseal volume, and deltoid tuberosity volume (WT and DKO only), were measured for 8-week-old and 6-8 mo-old mice. DICOM stacks were reconstructed in three-dimensions using OsiriX MD (Pixmeo, Switzerland) for visualization of frontal and sagittal planes. Reconstructed microCT images of the knee were three-dimensionally rendered using OsiriX MD to measure tibial slope. Briefly, the tibia and femur were

manually aligned in XY, YZ, and XZ planes using 3D volume rendering and 3D MPR and positioned using anatomical landmarks (Figure 4A). At least three angles were measured in both the medial and lateral compartments and averaged within each compartment (technical replicates) for each mouse.

For bone shape analyses, long bone scans (from 8 week and 6-8-mo-old mice, WT and DKO only) were reconstructed and analyzed using Dragonfly software (Object Research Systems, Montreal, Quebec). Bones were aligned along their respective neutral axes. Once aligned, a "Box Form" was created around each long bone of interest. Using the "Extract Structural Grid" function, the bone of interest was realigned and extracted. From the realigned version of each long bone of interest, lengths were measured between the most proximal point of the proximal epiphysis and the most distal point of the distal epiphysis. Volumetric data was collected using a "clip box" generated in Dragonfly to isolate the deltoid tuberosity (DT), lateral supracondylar ridge (LSR), and entire humerus for each sample. A threshold was defined to include only bone voxels for the DT and LSR. The "Split at Otsu" function was used to extract bone voxels for the entire humerus. The "Bone Analysis" function in Dragonfly was then used to fill in the bone ROI and measure the total bone ridge volume.

Histology

After microCT scans were complete, limbs were decalcified in formic acid or 14% EDTA (Immunocal, StatLab, TX, USA) for 72 hr or 2 weeks, respectively. Tissues were processed for paraffin sectioning, sectioned at 7μm, stained with Toluidine Blue (StatLab, Texas, United States), and imaged using an upright bright field microscope (Zeiss Axio Imager 2, Thornwood, NY). Supraspinatus attachment width was approximated using Toluidine Blue-stained histological sections using Image J (31). Histological sections from knees of 3-4 week old mice (WT and DKO groups; n=3/genotype) were used for terminal deoxynucleotidyl transferase dUTP nick end labeling (TUNEL) to visualize cell apoptosis/death (Roche, Basel, Switzerland). Sections were counterstained with DAPI and visualized using epifluorescence (Nikon Eclipse Ni E800). The total number of nuclei and TUNEL+ cells were counted in cropped regions of cruciate ligament-bone attachments in each knee; both caudal and cranial cruciate attachments on the femur and tibia, when visible, were measured using the particle analyzer tool using Fiji (32). At least two ligament attachments were measured for each biological replicate. The percentage of TUNEL+ cells was calculated for each attachment and percentages of TUNEL+ cells for each attachment were averaged within each knee.

Transmission electron microscopy (TEM) of Achilles tendons

The Achilles tendons of adult WT and DKO mice (6-8 months of age; n = 3 per genotype) were dissected and fixed for 2 weeks in a 2% glutaraldehyde, 2% paraformaldehyde solution buffered to pH 7.4 with 0.1M sodium cacodylate. Tendons were cut in the transverse plane from the proximal tendon and imaged to visualize collagen fiber diameters and tendon ultrastructure (Zeiss Libra 120 Transmission Electron Microscope; 120kV, 0.34nm point to point resolution, and Gatan Ultrascan 1000 CCD camera, Pleasanton, CA). Fiber area, fiber diameter, number of fibers, and fiber density were measured using automated segmentation of at least three (3) technical replicates per sample in Dragonfly (Object Research Systems,

Montreal, Quebec). Only two WT tendons were included in the analysis (with at least 3 technical replicates for TEM sections) due to poor infiltration of fixative.

Statistical Analysis

All statistical comparisons, including descriptive statistics, and graphical representation of data were performed using Prism 8.4.3 or later versions (Graphpad Software LLC, San Diego, CA). Two-way ANOVAs with repeated measures by region were used to compare tibial slopes (genotype, medial/lateral), epiphyseal volumes (genotype, age), and tibial and humeral length (genotype, age). Due to low sample size for R2cKO (n = 2), statistical comparisons were used to compare WT and DKO groups only and not statistically compared between single FGFR mutants. TUNEL-positive cell ratios were compared using an unpaired t-test of within-sample averages.

Acknowledgements

This research was supported by the Eunice Kennedy Shriver National Institute of Child Health & Human Development of the National Institutes of Health under award numbers R01AR079367 (MLK), K12HD073945 (MLK), R03HD094595 (MLK), and R01HD049808 and R01AR079246 (DMO); an Institutional Development Award (IDeA) from the National Institute of General Medical Sciences of the National Institutes of Health under award number P30GM103333; the National Institute of Arthritis and Musculoskeletal and Skin Diseases under award numbers P30AR057235 (WUSTL Musculoskeletal Research Center) and P30AR069620 (Michigan Integrative Musculoskeletal Health Core Center), and the University of Delaware Research Foundation (MLK). EG was supported by the University Doctoral Fellowship Award, ALS was supported by Delaware Space Grant Consortium, and EP was supported by the University of Michigan UROP. Microscopy access was supported by grants from the NIH-NIGMS (P20 GM103446), the NSF (IIA-1301765), and the State of Delaware. Special thanks to Shannon Modla and Jean Ross for assistance with electron microscopy, and to Christopher Price, PhD, for assistance with joint shape measurements from microCT.

References

1. Benjamin M, Ralphs JR. Entheses--the bony attachments of tendons and ligaments. Ital J Anat Embryol. 2001;106(2 Suppl 1):151–7. [PubMed: 11729950]
2. Zelzer E, Blitz E, Killian ML, Thomopoulos S. Tendon-to-bone attachment: From development to maturity. Birth Defects Research Part C: Embryo Today: Reviews. 2014 Mar;102(1):101–12. [PubMed: 24677726]
3. Locke RC, Abraham AC, Killian ML. Orthopedic Interface Repair Strategies Based on Native Structural and Mechanical Features of the Multiscale Enthesis. ACS Biomaterials Science & Engineering. 2016 Jan;3(11):2633–43. [PubMed: 32832593]
4. Thomopoulos S, Genin GM, Galatz LM. The development and morphogenesis of the tendon-to-bone insertion What development can teach us about healing. Journal of musculoskeletal & neuronal interactions. 2010;10(1):35. [PubMed: 20190378]
5. Liu Y, Schwartz AG, Birman V, Thomopoulos S, Genin GM. Stress amplification during development of the tendon-to-bone attachment. Biomechanics and Modeling in Mechanobiology. 2014 Oct;13(5):973–83. [PubMed: 24370852]
6. Liu YX, Thomopoulos S, Birman V, Li JS, Genin GM. Bi-material attachment through a compliant interfacial system at the tendon-to-bone insertion site. Mechanics of Materials. 2012 Jan;44:83–92.
7. Blitz E, Sharir A, Akiyama H, Zelzer E. Tendon-bone attachment unit is formed modularly by a distinct pool of Scx - and Sox9 -positive progenitors. Development. 2013;140(13):2680–90. [PubMed: 23720048]
8. Blitz E, Viukov S, Sharir A, Shwartz Y, Galloway JL, Pryce BA, et al. Bone Ridge Patterning during Musculoskeletal Assembly Is Mediated through SCX Regulation of Bmp4 at the Tendon-Skeleton Junction. Developmental Cell. 2009;17(6):861–73. [PubMed: 20059955]

9. Felsenthal N, Rubin S, Stern T, Krief S, Pal D, Pryce BA, et al. Development of migrating tendon-bone attachments involves replacement of progenitor populations. Development [Internet]. 2018 Dec 15 [cited 2020 Mar 25];145(24). Available from: https://dev.biologists.org/content/145/24/dev165381
10. Eyal S, Kult S, Rubin S, Krief S, Felsenthal N, Pineault KM, et al. Bone morphology is regulated modularly by global and regional genetic programs. Development. 2019 Jul 15;146(14):dev167882. [PubMed: 31221640]
11. Breidenbach AP, Aschbacher-Smith L, Lu Y, Dyment NA, Liu CF, Liu H, et al. Ablating hedgehog signaling in tenocytes during development impairs biomechanics and matrix organization of the adult murine patellar tendon enthesis. Journal of Orthopaedic Research. 2015 Aug;33(8):1142–51. [PubMed: 25807894]
12. Dyment NA, Breidenbach AP, Schwartz AG, Russell RP, Aschbacher-Smith L, Liu H, et al. Gdf5 progenitors give rise to fibrocartilage cells that mineralize via hedgehog signaling to form the zonal enthesis. Developmental Biology. 2015 Sep;405(1):96–107. [PubMed: 26141957]
13. Schwartz AG, Long F, Thomopoulos S. Enthesis fibrocartilage cells originate from a population of Hedgehog-responsive cells modulated by the loading environment. Development. 2015 Jan 1;142(1):196–206. [PubMed: 25516975]
14. Killian ML. Growth and mechanobiology of the tendon-bone enthesis. Seminars in Cell & Developmental Biology. 2022 Mar;123:64–73. [PubMed: 34362655]
15. Nowlan NC, Sharpe J. Joint shape morphogenesis precedes cavitation of the developing hip joint. J Anat. 2014 Apr;224(4):482–9. [PubMed: 24266523]
16. Nowlan NC, Murphy P, Prendergast PJ. A dynamic pattern of mechanical stimulation promotes ossification in avian embryonic long bones. Journal of Biomechanics. 2008;41(9):249–58. [PubMed: 18005973]
17. Nowlan NC, Bourdon C, Dumas G, Tajbakhsh S, Prendergast PJ, Murphy P. Developing bones are differentially affected by compromised skeletal muscle formation. Bone. 2010 May;46(5):1275–85. [PubMed: 19948261]
18. Eyal S, Blitz E, Shwartz Y, Akiyama H, Schweitzer R, Zelzer E. On the development of the patella. Development. 2015 May 15;142(10):1831–9. [PubMed: 25926361]
19. Shwartz Y, Viukov S, Krief S, Zelzer E. Joint Development Involves a Continuous Influx of Gdf5-Positive Cells. Cell Rep. 2016 21;15(12):2577–87. [PubMed: 27292641]
20. Sotiriou V, Rolfe RA, Murphy P, Nowlan NC. Effects of Abnormal Muscle Forces on Prenatal Joint Morphogenesis in Mice. J Orthop Res. 2019;37(11):2287–96. [PubMed: 31297860]
21. Kahn J, Shwartz Y, Blitz E, Krief S, Sharir A, Breitel Dario A, et al. Muscle Contraction Is Necessary to Maintain Joint Progenitor Cell Fate. Developmental Cell. 2009 May;16(5):734–43. [PubMed: 19460349]
22. Parisi C, Chandaria VV, Nowlan NC. Blocking mechanosensitive ion channels eliminates the effects of applied mechanical loading on chick joint morphogenesis. Philos Trans R Soc Lond, B, Biol Sci. 2018 24;373(1759).
23. Ornitz DM, Marie PJ. Fibroblast growth factors in skeletal development. Curr Top Dev Biol. 2019;133:195–234. [PubMed: 30902253]
24. Smith SM, Shu C, Melrose J. Comparative immunolocalisation of perlecan with collagen II and aggrecan in human foetal, newborn and adult ovine joint tissues demonstrates perlecan as an early developmental chondrogenic marker. Histochem Cell Biol. 2010 Sep;134(3):251–63. [PubMed: 20690028]
25. Karuppaiah K, Yu K, Lim J, Chen J, Smith C, Long F, et al. FGF signaling in the osteoprogenitor lineage non-autonomously regulates postnatal chondrocyte proliferation and skeletal growth. Development. 2016 15;143(10):1811–22. [PubMed: 27052727]
26. McKenzie J, Smith C, Karuppaiah K, Langberg J, Silva MJ, Ornitz DM. Osteocyte Death and Bone Overgrowth in Mice Lacking Fibroblast Growth Factor Receptors 1 and 2 in Mature Osteoblasts and Osteocytes. J Bone Miner Res. 2019 Sep;34(9):1660–75. [PubMed: 31206783]
27. Hung IH, Yu K, Lavine KJ, Ornitz DM. FGF9 regulates early hypertrophic chondrocyte differentiation and skeletal vascularization in the developing stylopod. Developmental Biology. 2007 Jul;307(2):300–13. [PubMed: 17544391]

28. Hung IH, Schoenwolf GC, Lewandoski M, Ornitz DM. A combined series of Fgf9 and Fgf18 mutant alleles identifies unique and redundant roles in skeletal development. Developmental Biology. 2016 Mar;411(1):72–84. [PubMed: 26794256]
29. Leek CC, Soulas JM, Bhattacharya I, Ganji E, Locke RC, Smith MC, et al. Deletion of Fibroblast growth factor 9 globally and in skeletal muscle results in enlarged tuberosities at sites of deltoid tendon attachments. Developmental Dynamics. 2021;250(12):1778–95. [PubMed: 34091985]
30. Roberts RR, Bobzin L, Teng CS, Pal D, Tuzon CT, Schweitzer R, et al. FGF signaling patterns cell fate at the interface between tendon and bone. Development. 2019 02;146(15).
31. Schneider CA, Rasband WS, Eliceiri KW. NIH Image to ImageJ: 25 years of image analysis. Nat Methods. 2012 Jul;9(7):671–5. [PubMed: 22930834]
32. Schindelin J, Arganda-Carreras I, Frise E, Kaynig V, Longair M, Pietzsch T, et al. Fiji: an open-source platform for biological-image analysis. Nat Methods. 2012 Jul;9(7):676–82. [PubMed: 22743772]
33. Chen J, Shi Y, Regan J, Karuppaiah K, Ornitz DM, Long F. Osx-Cre Targets Multiple Cell Types besides Osteoblast Lineage in Postnatal Mice. Tjwa M, editor. PLoS ONE. 2014 Jan 15;9(1):e85161. [PubMed: 24454809]
34. Mizoguchi T, Pinho S, Ahmed J, Kunisaki Y, Hanoun M, Mendelson A, et al. Osterix marks distinct waves of primitive and definitive stromal progenitors during bone marrow development. Dev Cell. 2014 May 12;29(3):340–9. [PubMed: 24823377]
35. Ono N, Ono W, Nagasawa T, Kronenberg HM. A subset of chondrogenic cells provides early mesenchymal progenitors in growing bones. Nat Cell Biol. 2014 Dec;16(12):1157–67. [PubMed: 25419849]
36. Robinson KA, Sun M, Barnum CE, Weiss SN, Huegel J, Shetye SS, et al. Decorin and biglycan are necessary for maintaining collagen fibril structure, fiber realignment, and mechanical properties of mature tendons. Matrix Biol. 2017;64:81–93. [PubMed: 28882761]
37. Reigle KL, Di Lullo G, Turner KR, Last JA, Chervoneva I, Birk DE, et al. Non-enzymatic glycation of type I collagen diminishes collagen-proteoglycan binding and weakens cell adhesion. J Cell Biochem. 2008 Aug 1;104(5):1684–98. [PubMed: 18348167]
38. Sweeney SM, Guy CA, Fields GB, Antonio JDS. Defining the domains of type I collagen involved in heparin- binding and endothelial tube formation. Proceedings of the National Academy of Sciences. 1998 Jun 23;95(13):7275–80.
39. Ornitz DM, Legeai-Mallet L. Achondroplasia: Development, pathogenesis, and therapy. Dev Dyn. 2017;246(4):291–309. [PubMed: 27987249]
40. Naski MC, Wang Q, Xu J, Ornitz DM. Graded activation of fibroblast growth factor receptor 3 by mutations causing achondroplasia and thanatophoric dysplasia. Nat Genet. 1996 Jun;13(2):233–7. [PubMed: 8640234]
41. Unger S, Bonafé L, Gouze E. Current Care and Investigational Therapies in Achondroplasia. Curr Osteoporos Rep. 2017;15(2):53–60. [PubMed: 28224446]

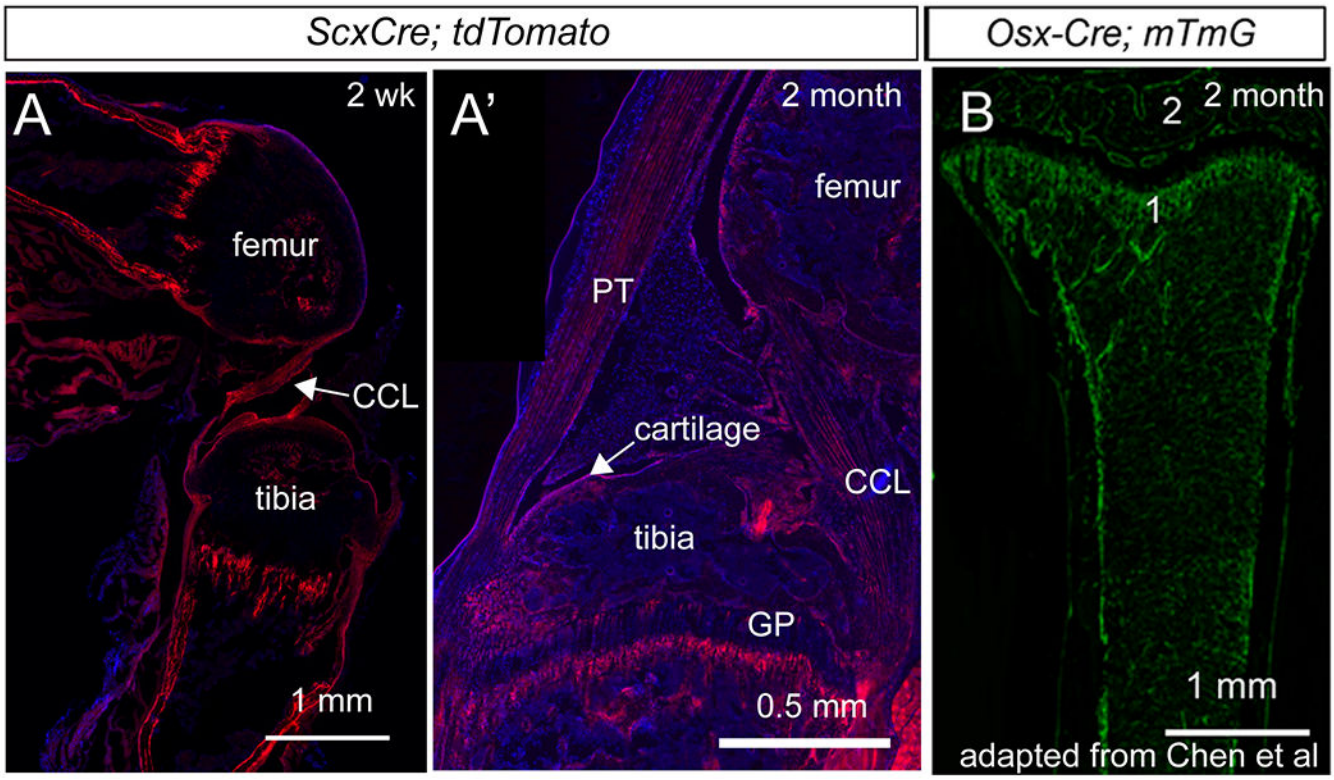

Figure 1. Lineage tracing of ScxCre.

Lineage tracing (ScxCre; *ROSA*^{tdTomato} reporter shown in red) of ScxCre at (A) 2 weeks of age and (A') 2 months of age. Scx-lineage cells were identified in tendon (e.g., PT = patellar tendon), ligament (e.g., CCL = cranial cruciate ligament), articular cartilage, and the primary spongiosa of the growth plate (GP). (B) Previously reported lineage tracing with Osx-Cre (Osx-Cre; *ROSA*^{mTmG}, GFP reporter shown in green) at 2 months of age (33). 1 = trabecular bone of the growth plate and 2 = secondary ossification center.

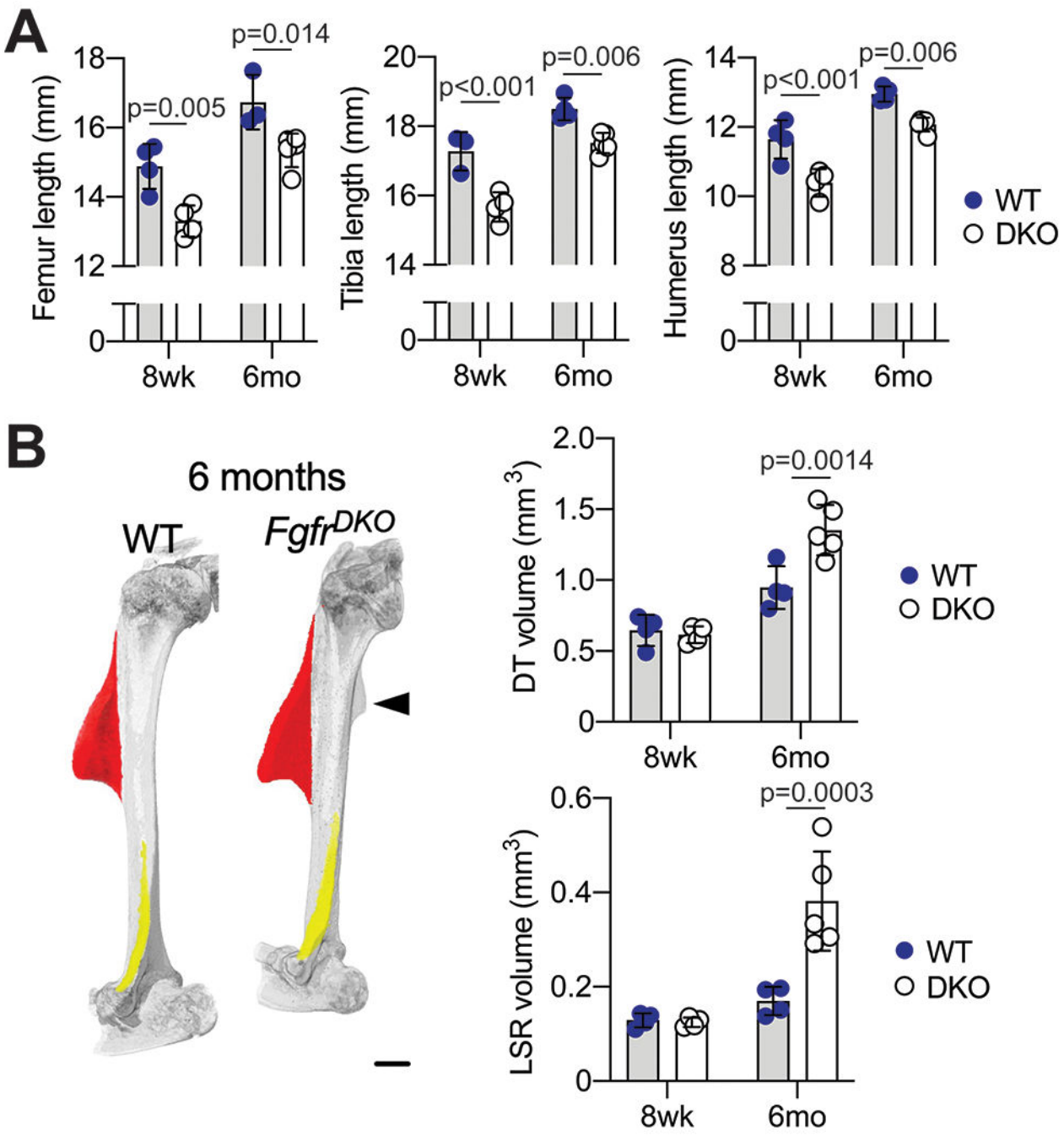

Figure 2. DKO mice had shorter bones with larger tuberosities.

(A) Long bone lengths (femur, tibia, and humerus) in DKO mice were significantly shorter at 8 weeks and 6 months (mo) compared to age-matched WT mice. (B) Superstructure volumes, visualized in representative microCT reconstructions of 6 months old WT and DKO humeri, were significantly larger in DKO mice compared to age-matched WT mice. Pseudo-colored structures show the representative regions used to measure volumes of the deltoid tuberosity (DT) in red, and the lateral supracondylar ridge (LSR) in yellow. Scale bar

= 1mm. Arrowhead = teres major attachment site. Length and volume data compared using ordinary two-way ANOVAs with Sidak's multiple comparisons tests.

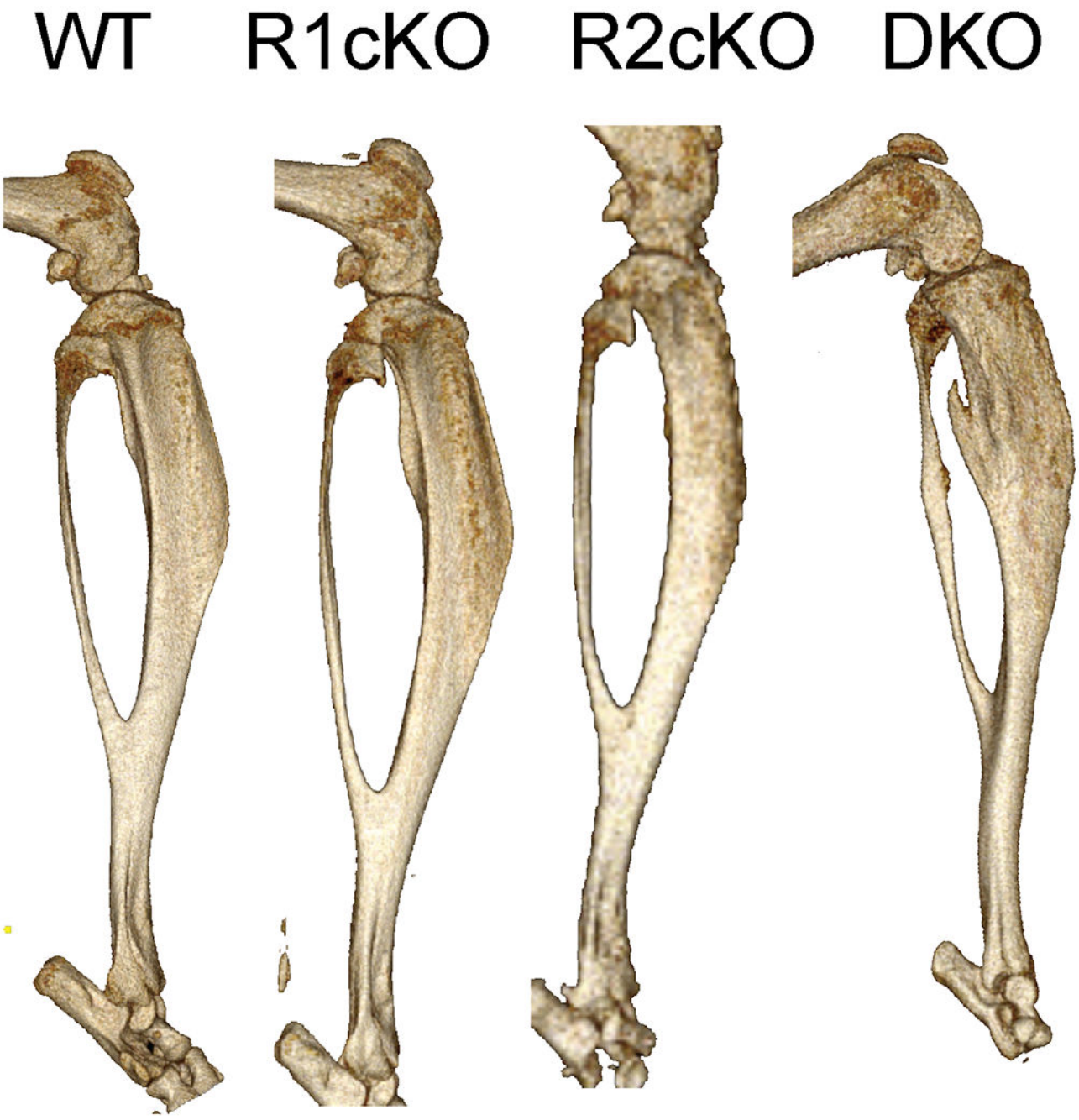

Figure 3. Visual representation of tibiae from adult DKO mice, which were shorter compared to WT littermates.

MicroCT reconstructions of tibia from WT, *Fgfr1* cKO, *Fgfr2* cKO, and DKO mice at 6-8 months of age. Images to scale; quantified data presented in Figure 2.

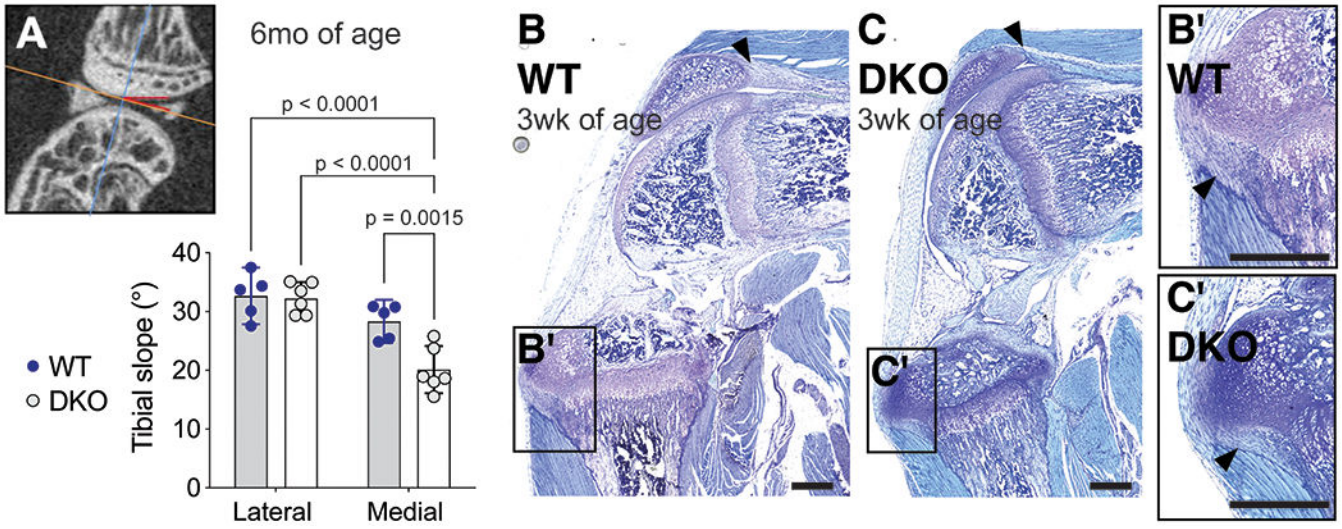

Figure 4. Decreased tibial slope and smaller groove of Ranvier in DKO mice.

(A) DKO mice had decreased medial tibial slope compared to WT mice at 6 months of age. Knee morphology at 3 weeks of age for (B) WT and (C) DKO showed marked differences in the morphology of the quadriceps tendon (black arrows) and (B', C') the groove of Ranvier (black arrows), which were smaller in DKO mice. Scale bar = 100μm. Data shown are mean ± 95% CI. Two-way ANOVA (repeated measures for lateral/medial compartment).

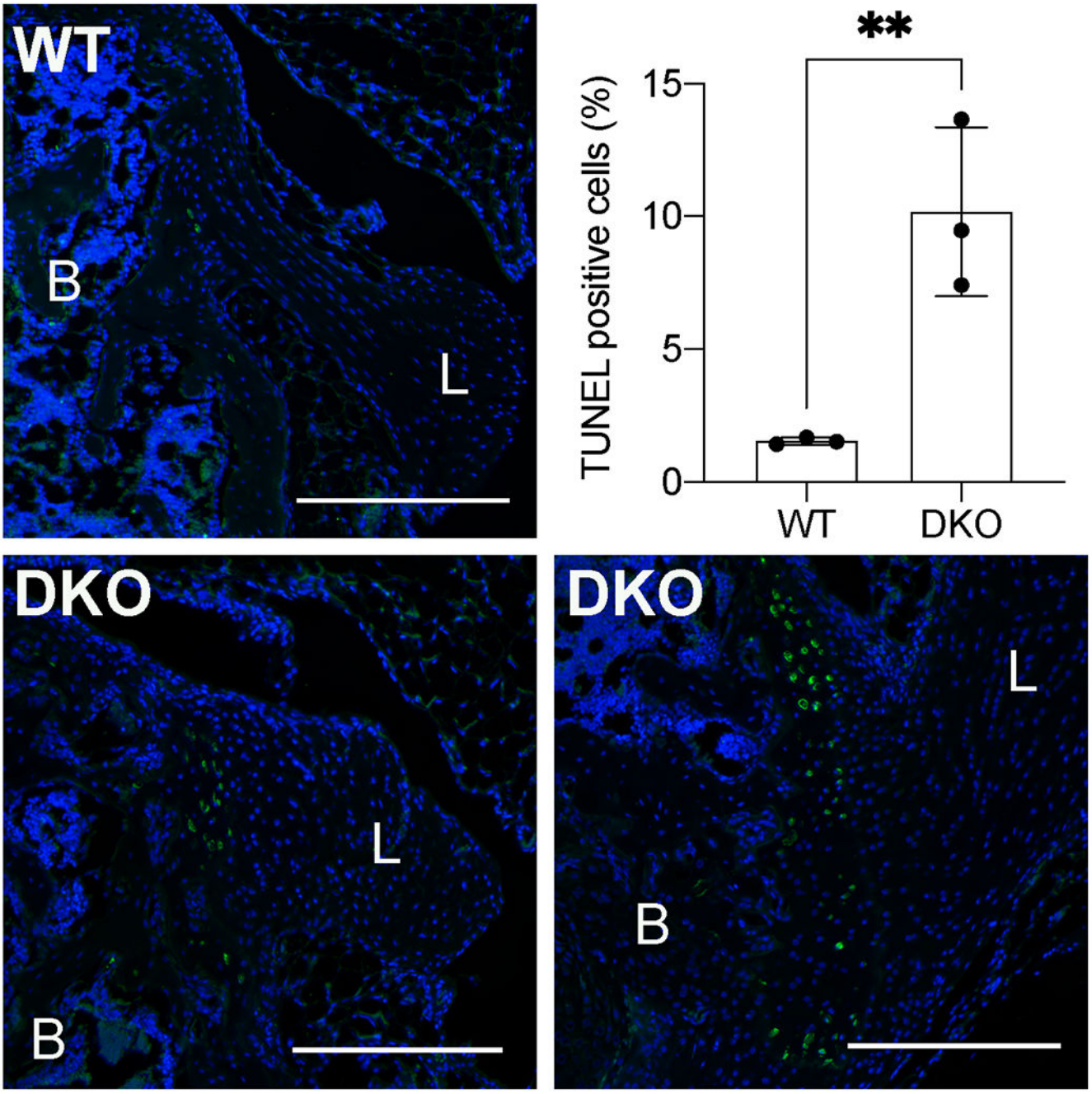

Figure 5. Increased cell death in DKO ligament entheses at 3 weeks of age.

Cruciate ligament attachments of WT knees had relatively low cell death, marked by TUNEL+ staining, compared to similar attachments in DKO knees. DKO ligament entheses had significantly higher rates of TUNEL+ cells compared to age-matched WT entheses. Ligament = L, bone = B. Scale bar = 250μm. Data represented are mean ± SD. ** p = 0.0246; unpaired t-test (two-tailed).

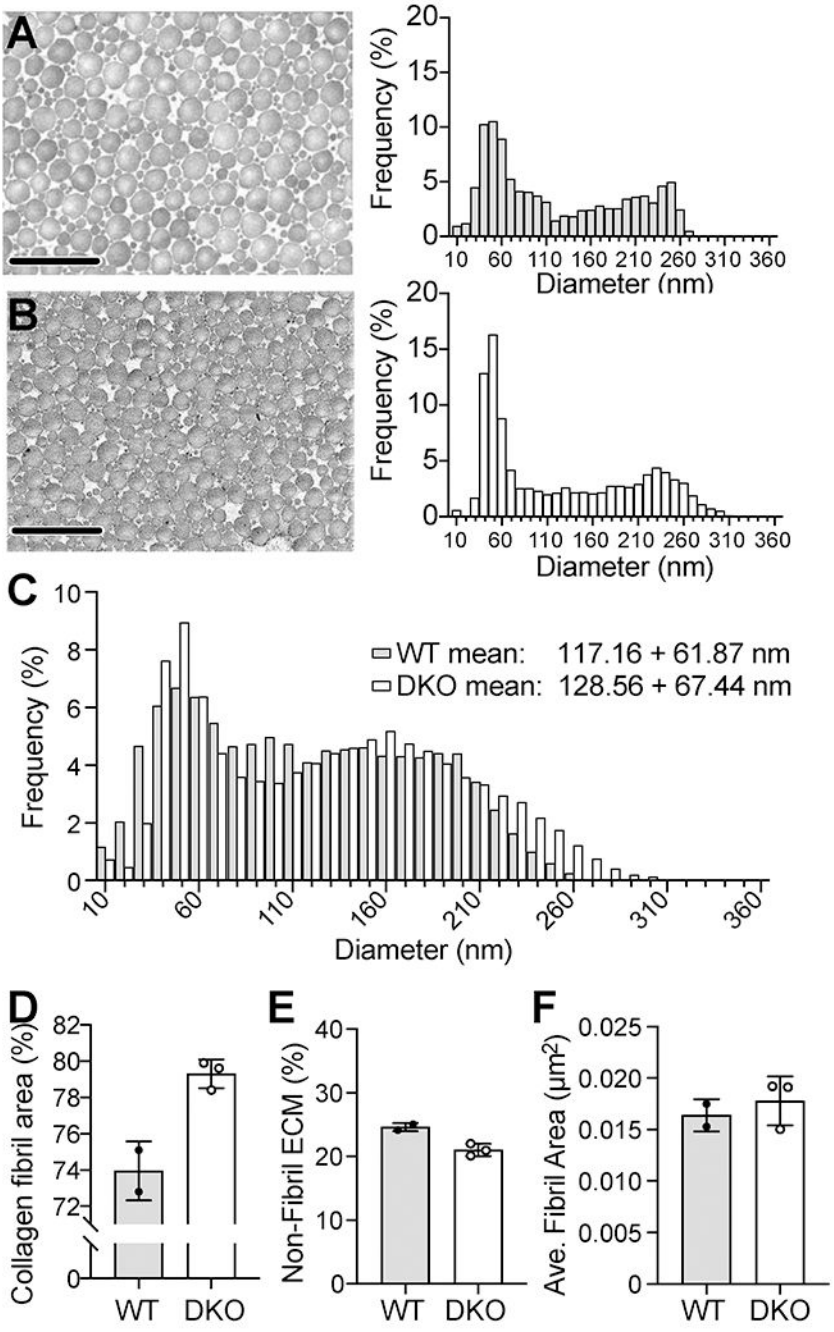

Figure 6. Collagen fibril ultrastructure of the Achilles tendons of WT and DKO mice.

Transmission electron micrographs and representative histograms of frequency distribution of fibril diameter (10 nm increments) of (A) WT and (B) DKO tendons (scale bar = 1μm). (C) Overlaid histogram of representative histograms for WT and DKO mice with average fibril diameters and standard deviations. (D) Collagen fibril area (%) was calculated for field of views and (E) non-fibril extracellular matrix area was measured as the entire area of the

field of view excluding collagen fibrils. (F) Average fibril area (μm^2) was measured using a watershed function in Dragonfly.